Journal of Geophysical Research: Solid Earth

RESEARCH ARTICLE
10.1029/2018JB015507

Hybridization Melting Between Continent-Derived Sediment and Depleted Peridotite in Subduction Zones

Yu Wang[1,2] and Stephen F. Foley[2]

[1]State Key Laboratory of Isotope Geochemistry, Guangzhou Institute of Geochemistry, Chinese Academy of Sciences, Guangzhou, China, [2]ARC Centre of Excellence for Core to Crust Fluid Systems/GEMOC, Department of Earth and Planetary Sciences, Macquarie University, Sydney, New South Wales, Australia

Key Points:
- The involvement of peridotite significantly affects the mobility of MREE, HREE, and transition elements during interaction between subducted sediments and mantle
- The hybridization process may account for characteristic geochemical features observed in Mediterranean postcollisional potassium-rich magmas
- Phlogopite is not necessarily required in the source to produce magmas with moderately high K_2O contents (3–5 wt%)

Supporting Information:
- Supporting Information S1

Correspondence to:
Y. Wang,
wangyu@gig.ac.cn

Citation:
Wang, Y., & Foley, S. F. (2018). Hybridization melting between continent-derived sediment and depleted peridotite in subduction zones. *Journal of Geophysical Research: Solid Earth*, *123*. https://doi.org/10.1029/2018JB015507

Received 17 JAN 2018
Accepted 6 APR 2018
Accepted article online 17 APR 2018

Abstract To better constrain the processes by which subducted continent-derived sediment and the overlying mantle wedge react to produce hybrid magmas, we have performed a series of high-pressure interaction experiments involving a phyllitic metasediment and a depleted peridotite (dunite) from the Mediterranean section of the Alpine-Himalayan orogenic belt at 2–3 GPa. Two different experimental methods were compared, namely, the reaction of separate, juxtaposed peridotite and metasediment blocks (reaction experiments) and capsules in which the two rocks were included as an intimately mixed powder before the experiments (mixed experiments). In reaction experiments, only the metasediment partially melted, and a marked, thin reaction zone dominated by orthopyroxene formed between the dunite and phyllite blocks. In contrast, a hybrid melt phase was found in all mixed experiments. Trace element analyses indicated that Cs, Rb, Ba, Th, U, Nb, Ta, Zr, and Hf were strongly incompatible, together with marked light rare earth element/heavy rare earth element fractionation. The reaction with peridotite can significantly affect the mobility of medium rare earth element, heavy rare earth element, and transition elements during sediment-mantle interaction, enriching them in hybrid melts. In addition, the nature of the sedimentary starting materials can considerably affect trace element behavior in resulting hybrid melts. There is a significant resemblance between the trace element distribution patterns of hybrid melts produced in our experiments and those of natural postcollisional potassium-rich volcanic rocks from the eastern Mediterranean region. The experiments show that phlogopite is not necessarily required in the source to produce the SiO_2-richer end of the range of K-rich magmas.

1. Introduction

The hypothesis that hydrous siliceous melts generated in the subducted oceanic crust would ascend and react with the overlying mantle peridotite (Nicholls & Ringwood, 1973) has long been considered a major mechanism in the petrogenesis of calc-alkaline magmas at depths of ~100–150 km (e.g., Blundy & Sparks, 1992; Prouteau et al., 2001; Tatsumi et al., 1986). In addition, abundant geochemical and isotopic evidence has been found to confirm the origin of many subduction-related magmas in sources consisting of mixed rock types (e.g., Arculus & Powell, 1986; Defant & Drummond, 1990; Kay, 1980; Prelević et al., 2005). Specifically, continental sedimentary material is recognized from trace element and isotope compositions to be involved during the generation of many volcanic melts in the Mediterranean region (Conticelli & Peccerillo, 1992; Peccerillo & Martinotti, 2006; Peccerillo et al., 1988; Prelević et al., 2008; Tommasini et al., 2011). This is most clearly demonstrated in alkaline compositions because the diagnostic chemical signals are not so strongly diluted by further melting of peridotite, indicating that the process may be common or even universal for more voluminous igneous rock types but is often overlooked because of the dilution effect (Foley & Pintér, 2018). In other areas not directly associated with accretionary tectonics, subducted sediments may be involved in the source. An example is the Gaussberg lamproite, which lies on the coast of eastern Antarctica far removed in time and space from any modern subduction zone, but has Pb isotopes compatible with sediments in the source (Murphy et al., 2002), requiring that continental crust must be stored for a considerable time within the mantle lithosphere and later reactivated. The investigation of processes that occur during subduction and during the preconditioning of the later volcanic source regions is essential for understanding subduction zone magmatism.

Several experimental studies have aimed at simulating the hybridization between subducted crust and mantle, and so at understanding the origin of a wide range of magmas produced at convergent plate boundaries.

Of particular significance, Sekine and Wyllie (1982a, 1982b, 1982c) used the $KAlSiO_4$-Mg_2SiO_4-SiO_2-H_2O system to experimentally investigate the hybridization between hydrous siliceous melts and peridotite at 2–3 GPa and to assess the effect of additional components by extending their systems with $NaAlSiO_4$, $CaMgSi_2O_6$, $CaAl_2Si_2O_8$, and Al_2O_3. These seminal works provided the first experimental evidence that the reaction products consist of olivine-free pyroxenite, made up of orthopyroxene + jadeitic clinopyroxene ± phlogopite ± garnet (Sekine & Wyllie, 1983). It was later shown that only small amounts of CaO are required to stabilize clinopyroxene in these pyroxenites (Melzer & Foley, 2000). In addition, a few studies focusing on slab-derived rhyodacitic melt and peridotite produced rhyolites, dacites, and Mg-andesites (Prouteau et al., 2001; Rapp et al., 1999; Tatsumi, 2001), whereas others tested the interaction between melts of siliciclastic/carbonate sediment or mid-ocean ridge basalt (MORB)-eclogite/mélange and fertile peridotite at various pressure-temperature (P-T) conditions applicable to subduction zones (Bulatov et al., 2014; Castro & Gerya, 2008; Mallik & Dasgupta, 2012, 2013, 2014; Mallik et al., 2015). However, very few experimental studies of *natural*, *continent*-derived sediment and *depleted* peridotites have been carried out: most have been based on a primitive or fertile mantle composition. Moreover, except for a study by Bulatov et al. (2014), who investigated interaction between synthetic carbonated sediment and harzburgite at 7.5–12 GPa, no experimental studies have attempted to directly investigate trace element distribution during the hybridization process between continent-derived sediment and depleted peridotite, which leaves a large gap in our knowledge and understanding of trace element redistribution in subduction zones. Furthermore, the experimental conditions and the strongly depleted peridotite chosen here are relevant to shallow melting in a postcollisional environment such as the eastern Mediterranean (Prelević et al., 2013), where depleted, forearc peridotites are involved. This contrasts with most experimental studies, which have investigated higher pressure melting corresponding to Andean subduction situations.

In this study, we simulate hybridization between continental crust and depleted peridotite using two different techniques and determine the composition of partial melts and the identity of likely residual mineral assemblages resulting from the hybridization process. We investigate trace element partitioning during mantle-crust hybridization, assessing partition coefficients between residual phases and hybrid melts at 2–3 GPa. We show that potassium-rich melts could result from hybridization between continent-derived sediment and depleted peridotite at shallow depths without the need for residual phlogopite.

2. Experimental and Analytical Methods

2.1. Starting Materials

A natural quartz phyllite sample (11KP01) was chosen to represent typical continent-derived upper crustal sediment in the eastern Mediterranean area (Wang, Prelević, et al., 2017). This was preferred to choosing a global average sediment composition in order to study reactions as close as possible to those naturally occurring in the eastern Mediterranean area. For peridotite, a strongly depleted composition (harzburgite/dunite) is most appropriate for high levels of the upper mantle in arcs, since these rocks result from depletion at mid-ocean ridges. Therefore, a natural cpx-bearing dunite (ZD11-53) with a mineral assemblage of olivine (>95%) + spinel (~2%) + cpx (<1%) was chosen. It occurs as a lens within harzburgite in the Jinlu Profile of the Zedang ophiolite, Yarlung Zangbo suture zone (South Tibet, China), with porphyroblastic microstructure where large olivine porphyroblasts are set in a fine- to medium-grained matrix of olivine, spinel (chromite), and cpx. Compositions of the starting materials (SMs) are listed in Table 1.

Sample capsules were prepared using two different methods, namely, reaction and mixed experiments. For *reaction experiments*, the capsules were prepared by packing together phyllite and dunite powders with 1:1 weight ratio as juxtaposed blocks (metasediment on top of peridotite). For *mixed experiments*, phyllite and dunite powders were intimately mixed in 1:1 weight proportion and ground together well in an agate mortar under ethanol for 40 min to make the mixture as homogeneous as possible. After the ethanol fully evaporated, the mixture was heated in a furnace overnight then stored in a desiccator for later use.

2.2. Experimental Procedure

All experiments were performed in a modified Boyd-England design piston-cylinder apparatus (Boyd & England, 1960) at Macquarie University. Furnace assemblies (12.7-mm diameter) were made of graphite with cylindrical talc outer sleeve and pyrex® inner sleeve and BN inserts. Although this resulted in contamination of

Table 1
Major (wt%) and Trace (ppm) Element Compositions of Starting Materials

Locality	Kopaonik area, Serbia			Zedang area, South Tibet, China
Sample	11KP01			ZD11-53
Rock	Quartz-phyllite	GLOSS	UCC	Dunite
SiO_2	76.7	58.57	66	42.16
TiO_2	0.7	0.62	0.5	0.04
Al_2O_3	11.6	11.91	15.2	0.20
FeO_T	3.4	5.21	4.5	8.35
MnO	0.06	0.32	0.08	0.13
MgO	1.1	2.48	2.2	49.53
CaO	1.6	5.95	4.2	0.19
Na_2O	1.6	2.43	3.9	0.07
K_2O	1.9	2.04	3.4	0.00
Cr_2O_3	0.01	NA	NA	0.36
LOI	1.5			0.25
Sum	100.27			101.28
Mg#	37	46	47	91
Li	33	NA	20	2.2
Sc	13	13.1	13.6	4.0
Ti	4269	NA	2458	37
V	58	110	107	16
Cr	1362	78.9	83	1984
Mn	1147	NA	600	1011
Co	11	21.9	17	129
Ga	10	NA	17	0.43
Rb	54	57.2	112	0.003
Sr	288	327	350	0.30
Y	20	29.8	22	0.07
Zr	56	130	190	0.02
Nb	9.7	8.94	12	0.016
Cs	1.6	3.48	4.6	0.003
Ba	355	776	550	0.50
La	30	28.8	30	0.005
Ce	63	57.3	64	0.003
Pr	7.2	NA	7.1	0.001
Nd	28	27	26	0.003
Sm	5.6	5.78	4.5	0.001
Eu	1.1	1.31	0.88	0.001
Gd	4.6	5.26	3.8	0.003
Tb	0.68	NA	0.64	0.000
Dy	3.8	4.99	3.5	0.007
Ho	0.8	NA	0.8	0.002
Er	2.1	2.92	2.3	0.011
Tm	0.31	NA	0.33	NA
Yb	2	2.76	2.2	0.021
Lu	0.26	0.413	0.32	0.005
Hf	1.6	4.06	5.8	0.001
Ta	0.75	0.63	1.0	0.003
Th	8.4	6.91	10.7	0.001
U	1.5	1.68	2.8	0.008
Th/La	0.28	0.24	0.36	0.20
Nb/Yb	4.85	3.24	5.45	0.76
Sm/La	0.19	0.20	0.15	0.20
Rb/Sr	0.19	0.17	0.32	0.01

Note. Global subducted sediment (GLOSS) from Plank and Langmuir (1998); upper continental crust (UCC) from Taylor and McLennan (1995) and McLennan (2001).

one experimental charge with boron at the highest P-T conditions, no other trace elements were affected (e.g., Adam & Green, 2006; Green et al., 2000). A minus 10% correction for friction was applied to calibrate measured pressure (Adam & Green, 2006; Green et al., 1966). Temperatures were measured using Pt-$Pt_{90}Rh_{10}$ thermocouples and automatically controlled by an Electromax V single-loop controller. The sample was welded into a 4-mm diameter Ag_{70}/Pd_{30} capsule with a wall thickness of 0.2 mm, minimizing iron loss from the charge to the capsule. After run durations of up to 192 hr, experiments were quenched by switching off the heating current. After the recovery of the capsules, they were cut into two along their long axis and embedded into epoxy mounts. These pucks were ground flat and polished successively with 9, 3, and 1 μ diamond suspension and finally carbon coated for inspection by electron microprobe and trace element measurements.

2.3. Analytical Techniques

All analyses were obtained at Macquarie University. Major and minor elements were determined with a CAMECA SX-100 electron microprobe, using operating conditions of generally 15 kV accelerating voltage at a beam current of 20 nA, 10 s counting time for peaks and 5 s for each background. For mineral phases, a beam diameter of 1 μm was used, which was increased to 5 μm for the analysis of quenched melt areas. Trace elements were measured using laser ablation-inductively coupled plasma-mass spectrometry (ICP-MS), with a repetition rate of 5 Hz and laser energy at the sample of 5–6 J/cm^2, allowing data collection from individual grains for at least 40 s. Nitrogen was mixed with helium before ablated materials were introduced into the ICP-MS. Data were measured for 60 s plus 30 s background with beam sizes of 30 and 50 μm for most samples, 80 μm for some large-grained melt pools, and 15 and 20 μm for a few small-grained accessory phases and melt areas. For calibration, NIST SRM 610 was analyzed at the beginning and after every 20 sample measurements. The ablation positions were carefully chosen to avoid inclusions and overlaps with other phases, and time-resolved element signals were monitored during ablation to exclude extraneous phases and inclusions. Analytical uncertainty (one sigma) for a spot analysis was normally less than 10%. However, because of the rather small size, 1 sigma errors were generally larger for analyses of quenched melts than they were for crystals.

3. Results

Melt proportions in all experimental runs were obtained by the program ImageJ using scanning electron microscopy (SEM) images and mass balance calculations, and results of all analyses are presented in Table 2. SEM images of polished surfaces of the experimental charges are shown in Figure 1. The reaction experiments present a clear distinction between phyllite and dunite halves, with a reaction zone between them (Figures 1a and 1b). Hydrous melts only occur in the phyllite, whereas no melt could be identified in either the dunite or the reaction zone, indicating that the experimental conditions used here (1000°C, 2 and 3 GPa) were well above solidus of the phyllite but below that of dunite, and the reaction zone acted as a shield to prevent further interaction. In order to resolve the composition of melts produced by the hybridization reaction between melts of the phyllite and the dunite, a second series of

Table 2
Experimental Run Conditions and Products

Run no.	Method	P (GPa)	T (°C)	T_C (°C)	Hours	Phases (mode %)
2036	Reaction	2	1000	883	192	Dunite half: Ol (96), Cpx (2), *Chr* Phyllite half: M (42), Qrz (41), Alm-grt (12), Ky (2), *Zir*, *Apa*, *Rt* Interaction belt: Opx (2), *Prp-grt*
2037	Mixture	2	1000	933	192	Opx (75), M (23), Ol (5.5), *Chr*, *Prp-grt*, *Zir*, *Apa*, *Rt*
2038	Mixture	2	1100	942	168	Opx (71), M (28), *Chr*
139	Reaction	3	1000	1003	192	Dunite half: Ol (93), Chr (2), *Cpx* Phyllite half: M (31), Coe (44), Alm-grt (14), Ky (6), *Zir*, *Apa*, *Rt* Interaction belt: Opx (4), *Prp-grt*
140	Mixture	3	1000	871	192	Opx (71), M (14.5), Prp-grt (6), Coe (6), Cpx (1.5), *Zir*, *Chr*
141	Mixture	3	1100	936	168	Opx (66), M (18), Prp-grt (8), Coe (5), Cpx (2), *Zir*, *Chr*

Note. This table was adapted from Wang, Foley, et al. (2017). Phases in italics are accessory phases present in the run products in the range of 0–1 vol%. T_C denotes temperatures calculated by the two-pyroxene thermometer of Brey and Köhler (1990) with error of ±16°C. Mineral abbreviations: M, melt; Ol, olivine; Qrz, quartz; Alm-grt, almandine-rich garnet; Prp-grt, pyrope-rich garnet; Opx, orthopyroxene; Cpx, clinopyroxene; Chr, chromite; Coe, coesite; Ky, kyanite; Zir, zircon; Apa, apatite; Rt, rutile.

experiments (mixed experiments) were performed by mixing the phyllite and dunite powders intimately before sealing them in the experimental capsule. As expected, a hydrous melt phase resulting from hybridization occurred in all mixed experiments at the same pressure-temperature conditions as the reaction experiments, producing melt pools of sufficient size for analysis (Figures 1c and 1d). Besides hydrous melt, orthopyroxene and chromite were also present in all mixed experiments. Garnet, a SiO_2

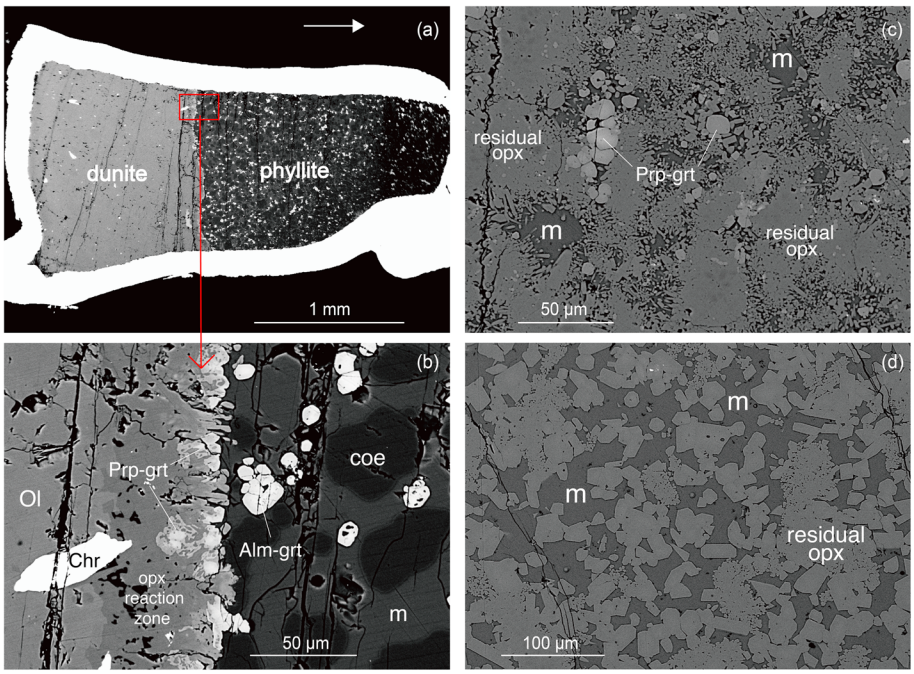

Figure 1. Representative back-scattered electron images of run products. (a) Reaction experiment (run 139; 1000°C, 3 GPa) showing clear distinction between phyllite and dunite halves with a thin reaction zone at the interface. Note that dunite half remained unmelted, while hydrous melts were present in phyllite half. The white arrow denotes the direction to the top of the capsule. (b) Enlargement of red square in (a) showing orthopyroxene-rich reaction zone, residual chromite, and two types of garnet coexisting. No new phases formed in the dunite half, indicating that it did not reach its solidus. (c) Mixed experiment 140 (1000°C, 3 GPa). Hybrid melts coexist with pyrope-rich garnet and orthopyroxene. (d) Mixed experiment 2038 (1100°C, 2 GPa), with the highest degree of melting. Only orthopyroxene and melt were present at higher degrees of melting. M, melt; Ol, olivine; Coe, coesite; Chr, chromite; Opx, orthopyroxene; Alm-grt, almandine-rich garnet; Prp-grt, pyrope-rich garnet. Adapted from Wang, Foley, et al. (2017).

phase, and clinopyroxene were seen as major phases in most of the runs with accessory zircon, apatite, and rutile, whereas kyanite only occurred in reaction experiments.

Experimental equilibrium and the reliability of melt compositions were established based on three criteria: (i) mineral phases were generally compositionally homogeneous with only minor zoning in garnet and clinopyroxene, (ii) there was no sign of quench crystals within the melt pools, and (iii) nominal experimental temperatures were reproduced by the two-pyroxene thermometer of Brey and Köhler (1990) in all experiments with insignificant discrepancy (Wang, Foley, et al., 2017).

3.1. Reaction Experiments

In the dunite half of the capsule, the phase assemblage remains the same as the SM (olivine + chromite + clinopyroxene) since there was no melting initiated. In the phyllite, hydrous melt occurs with 68 wt% SiO_2 and ~4 wt% K_2O, similar to compositions reported for melts of continental clastic sediment melts (Wang, Prelević, et al., 2017). A SiO_2 phase with variable grain size (5–80 μm) was present: quartz at 2 GPa and coesite at 3 GPa. In agreement with previous studies (Skora & Blundy, 2010), a clear morphological variation in the SiO_2 phase was observed, with coesite being more tabular and quartz appearing more rounded and irregular. The proportion of quartz/coesite increases with decreasing modal melting (42% to 31%).

Garnet occurred as idiomorphic and subhedral crystals (5–50 μm; Figure 1b); zoning was not common in garnets in the phyllite half (almandine-rich) but was more marked in garnets in the reaction zone (pyrope-rich). This was presumably due to slow intracrystalline diffusion and comparatively rapid crystal growth rates (Carlson, 2006; Chakraborty & Ganguly, 1991; Hickmott et al., 1987) because melt was used up in the reaction zone. As a result, garnet cores were enriched in Fe and rims in Mg and Ca. Minor elements in garnets such as Ti, P, and Na were also present in relatively high concentrations (0.60–1.27 wt% TiO_2, 0.14–0.19 wt% P_2O_5, and 0.06–0.24 wt% Na_2O). The coexistence of two chemically different garnet types in reaction runs has been found before in experimental studies of peridotite/melt reaction (Bulatov et al., 2014; Figure S1). Almandine-rich garnet with lower SiO_2 (~39 wt%), Al_2O_3, and MgO (8.5–11 wt%) but higher FeO_T (20–24 wt%), TiO_2, and P_2O_5 was produced during melting of the metasediment, whereas pyrope-rich garnet (41–43 wt% SiO_2, 18–22 wt% MgO, and 9.3–14 wt% FeO_T) was formed by hybridization process in the reaction zone.

The hybridization zone in reaction experiments was dominated by orthopyroxene (Figures 1a and 1b), which occurred as a belt along the dunite-phyllite boundary with width of ~10–50 μm. Compositions were enstatitic with ~33 wt% MgO, ~56 wt% SiO_2, and ~6.6 wt% FeO_T (Figure S2; Morimoto, 1988). Orthopyroxene acted as a chemical shield that intercepted any further infiltration of melt from the metasediment into the adjacent dunite. Only a trace amount of pyrope-rich garnet was formed in the hybridization zone, mostly occurring as anhedral grains with marked zonation (Figure 1b). Pressure exerted a slight effect on the reaction zone in terms of orthopyroxene fraction, which increased from 2 to 4% as pressure increased from 2 to 3 GPa at constant temperature of 1000°C.

Kyanite, rutile, apatite, and zircon occurred as accessory phases in the phyllite half. Kyanite occurred typically as acicular or needle-like grains; despite lengths of up to 50 μm, their widths were restricted (~2 μm), making them difficult to analyze. Rutile always occurred intergrown with almandine-rich garnet as tiny irregular braided crystal aggregates (2–20 μm). As the only TiO_2 phase, rutile plays a significant role in hosting trace elements (Wang, Prelević, et al., 2017). Likewise, although negligible in mode and size, zircon and apatite are extremely important accessory phases determining the distribution of many key trace elements during melting. Clinopyroxenes were only seen in the partially melted phyllite in one experiment (139, 1000°C, 3 GPa) as tiny anhedral tablets (~2 μm). These do not have a major effect on the residual compositions or melting behavior.

3.2. Mixed Experiments

There was no quartz in the mixed experiments. Coesite occurred in experiments at 3 GPa with similar composition and morphology to that described above. Pyrope-rich garnet was present in runs 140 and 141 with more subhedral and smaller grains (~2–40 μm) than those formed in reaction runs (Figure 1c). In run 2037 (1000°C, 2 GPa), only a trace amount of garnet was seen, whereas in run 2038 (1100°C, 2 GPa), garnet was eliminated during melting, indicating exhaustion slightly above 1000°C at 2 GPa. Chemically, garnets that formed in these hybridization experiments showed analogous composition to the pyrope-rich garnet in

the reaction zone of the first series of experiments, with pyrope content of ~65, almandine ~22, and grossular ~14, and had similar zoning characteristics. Chromite was present in all experiments, occurring as large anhedral grains (~10–60 μm) intergrown with orthopyroxene. Chromites show a consistent increase of Al_2O_3 and MgO contents and decrease of Cr_2O_3 and FeO_T as temperature increases from 1000 to 1100°C (Table S4).

Although olivine was found in one low-temperature experiment (run 2037), we interpret it as unmelted remnants from the dunite. No olivine survived in run 140 (lower melting degree, longer duration), and the composition of olivine in run 2037 was almost identical to that in the SM. No olivine was identified in any other experiment despite the dunite consisting of >95% olivine at the start of the experiments. Clinopyroxene occurred in runs at 1000 and 1100°C, 3 GPa but was eliminated at 2 GPa at the same temperature. Clinopyroxene also showed nearly the same diopsidic composition as in the unmelted dunite, with CaO, MgO, and FeO_T of ~24, 17, and 2 wt%, respectively (Figure S2).

Orthopyroxene dominated the solid phases in all four mixed experiments as idiomorphic tabular or lath-shaped crystals at 2 GPa, and anhedral tiny aggregate grains in runs with low degrees of melting at 3 GPa (Figures 1c and 1d). Orthopyroxenes in the mixed runs also showed consistently enstatitic composition (Mg# ~88%; Figure S2). As the degree of melting increases, the modal abundance of orthopyroxene drops slightly at both pressure conditions.

All melts in mixed experiments were high-potassium dacite or trachyte in composition with SiO_2 content ~68 wt% and K_2O ~4 wt%. No K-rich phase was present other than melt, which means that at the PT conditions in this study, potassium is contained exclusively in melts and not in any coexisting K-rich mineral such as mica (Hermann & Spandler, 2007; Thomsen & Schmidt, 2008). Several compositional differences could be recognized between hybrid and metasediment melts (Table S1 and Figure 2). First, the volatile content was lower in melts of metasediments than in hybrid melts, and second, the MgO content was lower in metamelts of metasediment than in hybrid melts (Figure 2e). For the hybrid melts, the degree of melting increased as pressure decreased at constant temperature. TiO_2, FeO_T, MgO, and CaO contents in melts increase with the degree of melting (Figure 2). Additionally, SiO_2 contents decrease at 3 GPa from 68.5 to 65.5 wt% but increase slightly at 2 GPa as temperature rises from 1000 to 1100°C. We attribute this to the presence of a SiO_2 phase (coesite) in mixed experiments at 3 GPa, which did not occur at 2 GPa, (e.g., Wang, Prelević, et al., 2017). Na_2O and K_2O contents in hybrid melts present similar variations, that is, for runs at 3 GPa they increase with temperature, while at 2 GPa they decrease (Figures 2g and 2h). The reason that hybrid melts show opposite Na_2O and K_2O compositional variations as temperature increases at differing pressures might be twofold: First, the error bars for both elements are relatively large, especially K_2O, and second, differing residue assemblages at 2 and 3 GPa might control the alkali variations. The latter should be better constrained in future experiments.

4. Discussion

4.1. Reaction Versus Mixed Experiments

Several previous studies have investigated subduction zone hybridization using either layered/sandwich or mixed rock methods (e.g., Bulatov et al., 2014; Castro & Gerya, 2008; Johnston & Wyllie, 1989; Mallik & Dasgupta, 2012, 2013, 2014; Mallik et al., 2015; Martin et al., 2012; Rapp et al., 1999; Sekine & Wyllie, 1982a, 1982b, 1983), but direct comparisons between these two experimental methods are rather rare. Recently, Mallik and Dasgupta (2012) examined the reaction between volatile-free MORB-eclogite and fertile peridotite using both methods, but at differing experimental conditions. The only available comparison is from Bulatov et al. (2014), who conducted melting experiments on GLOSS-like sediment (global subducted sediment) as well as GLOSS-peridotite interaction experiments, but did not perform mixed experiments.

In our reaction experiments, melting only took place in the metasediment half because the PT conditions applied were too low to reach the melting point of dunite. Therefore, melt infiltration from the phyllite was restricted to a thin boundary between the two rocks, where the reaction formed mostly orthopyroxene with minor garnet (Figure S3). In contrast, in mixed experiments, extensive hybridization melting could be recognized and documented because of the physical mixing of the two rocks prior to the experiment,

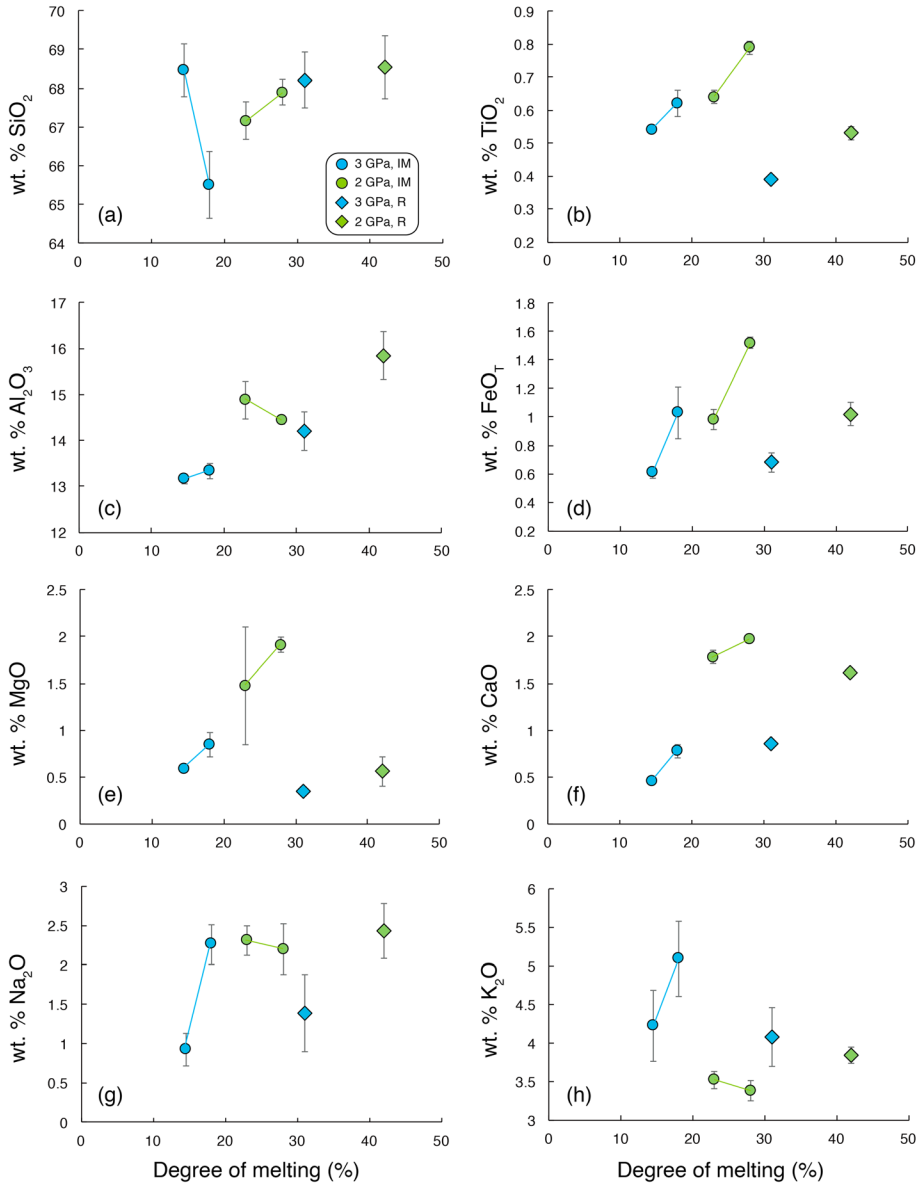

Figure 2. Composition of melts produced in this study (in wt%) as a function of the degree of melting. The green and blue lines illustrate the compositional variations for IM runs conducted at 2 and 3 GPa, respectively. IM, intimately mixed runs; R, reaction runs. The error bars indicate uncertainties of one standard deviation.

resulting in large areas of orthopyroxene together with well-distributed pools of hybrid melt. In the reaction zone, the two new phases orthopyroxene and pyrope-rich garnet were formed following equations (1) and (2), respectively:

$$\underset{\text{(forsterite)}}{Mg_2SiO_4} + \underset{\text{(melt)}}{SiO_2} \rightarrow \underset{\text{(enstatite)}}{2MgSiO_3} \quad (1)$$

$$\underset{\text{(melt)}}{3MgO} + \underset{\text{(alm–grt)}}{Fe_3Al_2Si_3O_{12}} \rightarrow \underset{\text{(melt)}}{3FeO} + \underset{\text{(prp–grt)}}{Mg_3Al_2Si_3O_{12}} \quad (2)$$

Orthopyroxenes formed in the thin reaction zone in reaction experiments and showed no major compositional variation in the mixed runs. Almandine-rich garnet occurred only in the phyllite half of reaction experiments, whereas pyrope-rich garnet equilibrated with orthopyroxene at the reaction zone as a result of

infiltration of melt from the metasediment. The same reaction occurred more completely in mixed experiments, evidenced by the Fe-rich core observed in some of the pyrope-rich garnets.

Normally, a layered geometry as used in the reaction hybridization experiments can constrain the reaction boundary between two different rocks well and provide a clear view of how melt infiltrates into the other rock, causing subsequent changes in modal mineralogy and composition. However, the differing solidus of the two rocks studied here makes it difficult to melt both rocks at the same PT conditions, and the formation of orthopyroxene and garnet rapidly exhausted the infiltrating melt, forming a barrier to melt migration and preventing the formation of a wide reaction zone.

The mixed geometry of the second experimental series assists the hybridization process between the two rocks and generates measurable pools of incipient hybrid melts even at low temperature. These experiments are more likely to correspond to the results of reaction in the natural environment because of the much longer time available. Mixed experiments allow characterization of the melt composition produced by hybridization but give only restricted information on the initial contact zone. Therefore, each method has its own pros and cons and the combination is especially informative; the comparison of both results enables a full understanding of the hybridization process. It should also be noted that in nature it is highly unlikely that the same 1:1 mixing ratio as in these experiments will occur, and hybridization processes that occur between continental crust and mantle in subduction zones cannot be naturally imitated within the time and length scales of a simple experiment.

4.2. Trace Element Partitioning

The trace element compositions of all phases with measurable size were obtained by laser ablation-ICP-MS and listed in Tables S5–10. All analyses were relatively homogeneous as shown by 1σ deviations on multiple spots, with typically ≤10% relative, with only a few exceptions where heterogeneities can be explained by small grain size or chemical zoning. We screened our data to eliminate those showing clear physical evidence (via SEM) of contamination by other phases or zoning. However, for some phases, only one analysis could be obtained, especially for accessory phases, so that the possibility of contamination of trace element analyses cannot be completely eliminated.

Comparison of partitioning results with published data, especially the work of Bulatov et al. (2014), who conducted similar sediment (synthetic materials similar to GLOSS)-peridotite (harzburgite mixture of natural olivine, orthopyroxene, and garnet from kimberlite-derived xenoliths) interaction experiments at 7.5–12 GPa and 900–1400°C, allows us to decode how trace elements will behave during hybridization melting at the interface between subducted sediment and mantle wedge at depths of 60–100 km, and during interaction at depths greater than 300 km (Tables S11–14). All experimental data compared here are within the Henry's law region, which applied for doped experiments (Green, 1994).

4.2.1. Garnet/Melt Partitioning

Although some pyrope-rich garnets were produced in reaction experiments, they might not have reached equilibrium due to the high rate of melting relative to more sluggish crystallization, which would result in incomplete partitioning. Therefore, here we only discuss those produced in mixed experiments to represent the pyrope-rich garnets. In this study, heavy rare earth element (HREE) are strongly compatible in both almandine-rich and pyrope-rich garnets, especially in almandine-rich garnets ($D_{HREE} \geq 10$; Figure 3a). Consequently, a clear positive slope for REE can be seen in garnet, denoting its strong HREE preference over light rare earth element (LREE; e.g., Johnson, 1998; Pertermann et al., 2004; Shimizu & Kushiro, 1975; van Westrenen et al., 2001). Although patterns are similar, garnets produced in the sediment-peridotite interaction experiments of Bulatov et al. (2014) show generally lower partition coefficients for incompatible elements, particularly those plotting to the left of Tm. Scandium, V, Cr, Mn, and Co are also compatible in all garnets ($\sim 1 < D < 10$). Despite the fact that most elements in the sediment-peridotite interaction experiments show lower partition coefficients than this study, Cr in pyrope-rich garnet is an exception, which results from buffering by chromite in this study. In contrast, large ion lithophile element (LILE) and high field strength element (HFSE; Th, U, Nb, Ta, Zr, and Hf; $0.01 < D < 1$) are consistently incompatible in all garnets from both this study and Bulatov et al. (2014). In our study, Sr is the most incompatible element in all garnets ($D_{Sr} = \sim 0.1$), whereas in the high-pressure garnets formed by both sediment melting and sediment-peridotite interaction (Bulatov et al., 2014), this feature is less pronounced with LREE (La, Ce, and Pr) exhibiting the strongest incompatibility. Zr and Hf show the most consistent partition coefficients between garnets and melts

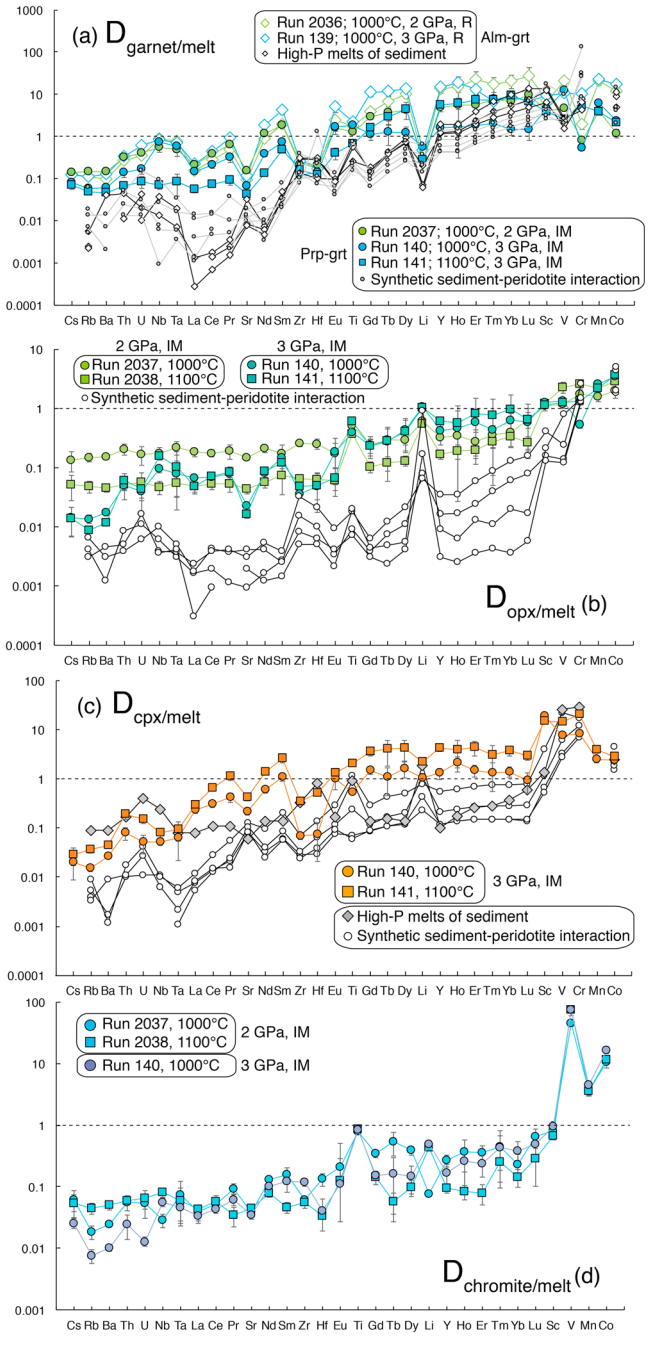

Figure 3. Mineral/melt trace element partition coefficients (D) from the experiments. (a–d) Garnet, orthopyroxene, clinopyroxene, and chromite, respectively. High-pressure sediment melting and sediment-peridotite interaction data from Bulatov et al. (2014). The error bars indicate propagated uncertainties as single standard deviations. Partition coefficients of most key elements in this study are higher than those in Bulatov et al. (2014) and also note the partitioning distinction between sediment melting and sediment-peridotite interaction. IM, intimately mixed runs; R, reaction runs.

(D = ~0.1) in all experiments. Noticeably, D_{Nb} and D_{Ta} in run 141 are markedly lower, most probably due to the exhaustion of rutile. Pressure exerts no significant effect on element partitioning in our experiments, whereas temperature affects partition coefficients dramatically. For elements from Cs to Hf, partition coefficients in run 140 (1000°C, 3 GPa) are considerably higher than those of run 141 (1100°C, 3 GPa), but this trend is reversed for elements from Gd to Lu (Figure 3a). Likewise, in both this study and Bulatov et al. (2014), sediment melting experiments give rise to almandine-rich garnets, whereas sediment-peridotite interaction experiments produce pyrope-rich garnets. Generally, almandine-rich garnets show stronger medium rare earth element (MREE) and HREE affinity than pyrope-rich ones in relative to LREE.

4.2.2. Orthopyroxene/Melt Partitioning

Generally, except for transition elements (Sc, V, Cr, Mn, and Co), all key elements are incompatible in orthopyroxene (Figure 3b), in agreement with many previous studies (e.g., Lee et al., 2007; Nielsen et al., 1992). However, when compared with similar experiments conducted on sediment-peridotite interaction, partition coefficients of almost all elements in orthopyroxenes obtained by Bulatov et al. (2014) at higher pressures are much lower (1–2 orders of magnitude) than those from this study, particularly for LREE. Exceptions are Rb, Li, Cr, and Co, which show closer partition coefficients to those in this study. There is a slight HREE preference in all orthopyroxenes during sediment-peridotite interaction melting. At 2 GPa, both D_{LILE} and D_{HFSE} give rather flat trends in this study, whereas at 3 GPa D_{LILE} and D_{HFSE} are markedly lower. At 2 GPa, partition coefficients of elements from Cs to Eu rise substantially as temperature increases from 1000 to 1100°C (Figure 3b). However, this difference in slope is not evident in runs at 3 GPa.

4.2.3. Clinopyroxene/Melt Partitioning

In agreement with previous studies, clinopyroxenes in this study exhibit partition coefficient patterns with slight HREE preference over LREE, peaking at around Ho (Foley et al., 1996; Hauri et al., 1994; Johnston & Schwab, 2004). However, differing from many previous works, $D_{cpx/melt}$ of *most* trace elements in this study show higher values than unity. Particularly, D_{HREE} are mostly slightly over 1, whereas D_{LREE} are less than 1 only for the lightest REE. This is probably related to the SiO_2-rich nature of the melts, as mineral/melt partition coefficients are generally higher where the melt is more polymerized (Nash & Crecraft, 1985). At 3 GPa, partition coefficients for many trace elements increase as temperature rises from 1000 to 1100°C (Figure 3c). Similar to garnet and orthopyroxene, almost all clinopyroxenes produced in this study show much higher partition coefficients than those at higher pressures from Bulatov et al. (2014) during sediment-peridotite interaction (Figure 3c). However, for synthetic sediment melting only, a remarkable feature is the high partition coefficients for elements from Cs to Hf (except for Sr). Cesium, Rb, Ba, Zr, and Hf are the most incompatible elements, while Sc, V, and Cr are most compatible in our clinopyroxenes.

4.2.4. Chromite/Melt Partitioning

As widely acknowledged in many previous studies, chromium-spinel is extremely depleted in incompatible trace elements (negligible concentrations far less than chondrite) and so plays an insignificant role for these elements in mantle processes despite its ubiquitous occurrence in the upper mantle (Glaser et al., 1999; Stosch, 1982). Although several works have pointed out the potential of chromite in hosting some HFSEs relative to REEs (Bodinier et al.,

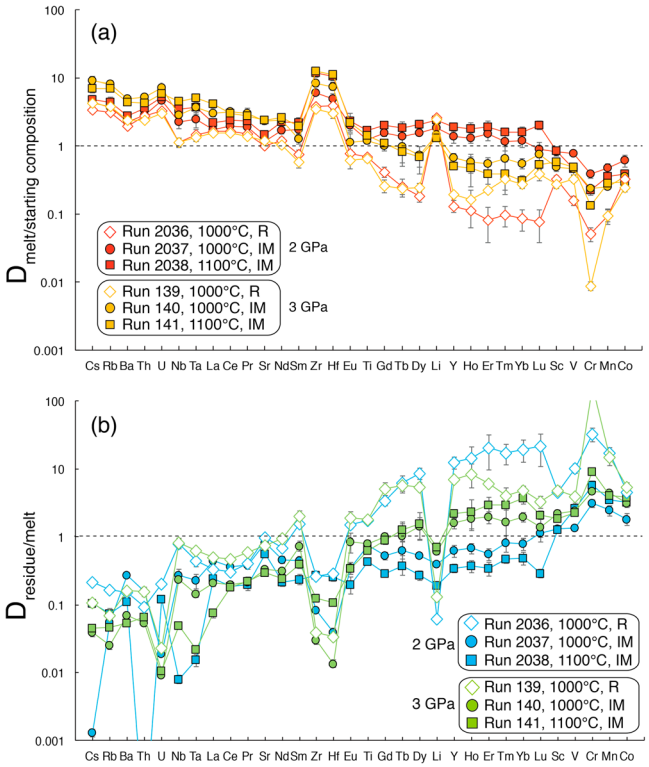

Figure 4. (a) Melt/starting material and (b) residue/melt trace element partitioning from this study. Note the mirrored patterns between the two diagrams and the clear distinction between melts of phyllite (R) and hybrid (IM) melts. R, reaction runs; IM, intimately mixed runs.

1996; Kelemen et al., 1993; McDonough et al., 1992), partition coefficients for these elements are only higher where there is a significant TiO_2 content in the spinel (Nielsen et al., 1994). In this study, all elements other than V, Mn, and Co, which show strong compatibility, are incompatible in runs 2037, 2038, and 140 (Figure 3d).

Because attention has concentrated mostly on the behavior of platinum-group elements in chromite (Brenan et al., 2012; Page & Barnes, 2009), there are few partitioning results for other trace elements to compare with our study. At 2 GPa, D values of elements from Pr to Lu (except for Sr, Ti, and Li) decrease as temperature increases from 1000 to 1100°C. At 1000°C, as pressure rises from 2 to 3 GPa, partition coefficients of most of the trace elements decrease except for Nb, Zr, Ti, Li, Yb, and transition elements (Sc, V, Mn, and Co). Therefore, both temperature and pressure could exert great effect on elemental partitioning of chromite. The exceptionally high D_V (45–76) indicates reducing conditions in the experiments, as vanadium is accommodated in spinels as V^{3+} (Horn et al., 1994).

4.2.5. Melt/Bulk Fractionation and Residue/Melt Partitioning

Partition coefficients between melt and bulk residue were calculated following the equation

$$D_i^{\text{residue/melt}} = \left(C_i^{\text{SM}} - X \times C_i^{\text{melt}}\right) / \left(C_i^{\text{melt}} - \text{X} \times C_i^{\text{melt}}\right) \quad (3)$$

where X is the melt proportion in weight percent and C_i^{SM} and C_i^{melt} are the abundances of a specific element i in SM and melt, respectively. For reaction experiments, because melting only occurred in the phyllite half, "residue" here refers to the residue of this half of the capsule with the minerals listed in Table 2.

Partitioning behavior is distinctly different for the two types of melts: the hybrid melt that interacted with Mg-rich phases and the other, direct melt of the phyllite that is equilibrated with less magnesian minerals. Generally, fractionation between phyllite melt and bulk rock is much stronger than for hybrid melt, except for Li. Zr and Hf are the most enriched elements in melts (D_{Zr} and D_{Hf} ~10), followed by LILE (Cs, Rb, and Ba), Th, U, Nb, and Ta with $D_{melt/SM} > 1$. Cr is the most immobile element during melting, along with Sc and other transition elements (V, Mn, and Co). Phyllite melts tend to favor LREE over HREE (evidenced by downward slopes from left to right for REE), considerably more than do hybrid melts (Figure 4a). Almost all the above characteristics of melts are well mirrored in residue-melt partitioning in Figure 4b. The residue of hybridization runs shows similar partitioning features ($D_{residue/melt}$ ~ 1) with hybrid melt except for LILE and HFSE, whereas the residue of phyllitic melts exhibits marked preference of elements from Eu to Lu. Neither temperature nor pressure seems to exert a consistent effect on partition coefficients in either type of experiment. The equilibrium mineral assemblage is the main factor that controls D value.

4.3. Trace Element Behavior During Hybridization Between Sediment-Derived Melt and Mantle Peridotite in Subduction Zones

The production of melt areas in mixed experiments makes scrutinizing element distribution during subducted sediment/mantle wedge interaction at shallow depth in subduction zones possible and also enables us to compare the difference between these hybrid melts and those produced by melting of the phyllite alone in the reaction experiments. Although several published studies have been directed toward mantle hybridization (e.g., Castro & Gerya, 2008; Mallik et al., 2015; Rapp et al., 1999; Sekine & Wyllie, 1982a), few have studied trace element distribution (Mallik et al., 2016). Here we compare our data only with other studies conducted on natural rocks to avoid complications with unnatural levels of trace element doping.

Trace element distribution patterns in melts produced by direct melting of phyllite and by phyllite-dunite interaction exhibit great similarity for LILE, HFSE, and LREE, whereas MREE, HREE, and transition elements are more depleted in direct melts of sediment than in hybrid melts (Figure 5). This indicates that the

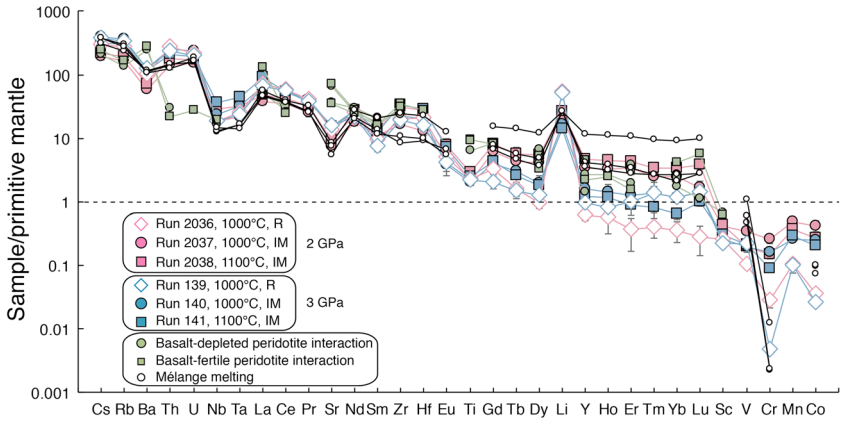

Figure 5. Primitive mantle normalized trace element compositions of experimental melts. Data for basalt-depleted/fertile peridotite interaction from Rapp et al. (1999), mélange melting data from Castro et al. (2010), and primitive mantle values from Palme and O'Neill (2003). R, reaction runs; IM, intimately mixed runs.

reaction with peridotite can significantly affect the mobility of MREE, HREE, and transition elements during the sediment-mantle interaction, enriching them in hybrid melts. Rapp et al. (1999) found similar element behavior except for Th, U, and Sr (Figure 5; basalt-peridotite interaction). In interaction experiments with both depleted and fertile peridotites, Th and U exhibit around an order of magnitude lower concentrations and Sr shows ~10 times higher concentrations than in this study. We attribute this to the different SMs used in the two studies: phyllite contains much higher Th (8.4 ppm) and U (1.5 ppm) and lower Sr (288 ppm) contents than in Rapp et al.'s basalt (0.33, 0.07, and 359 ppm for Th, U, and Sr, respectively). For melting of mélange involving oceanic crust (MORB-derived amphibolite) and sediments (mica-rich metagraywacke; Castro et al., 2010), similar Th and U enrichments as well as Sr depletion can be seen (Figure 5), showing again that the differing nature of the sedimentary SMs can considerably affect the trace element behavior in resulting hybrid melts. The sediment-peridotite (melt/rock) ratio at the slab-mantle interface where infiltration melting occurs will thus be a key factor in controlling elemental behavior in subduction zones. Changes of phase proportions and residual phase assemblages during hybridization between sediment and peridotite are the principal cause of chemical variations in melts. In melts of mélange where sedimentary material and MORB are involved, most elements behave in a similar manner to that in melts of phyllite: exceptions are the HREE, which are more enriched analogous to the hybrid melts, implying that sediment-MORB interaction can also increase the enrichment of HREE in the melts. Hybridization processes at shallow mantle depths involving either sediment-MORB or sediment-peridotite are thus instrumental in producing melts with enriched incompatible elements, especially HREE (Figures 4a and 5).

Apart from the similar trace element distributions, there are several chemical distinctions and affinities that characterize the two types of melt. First, Zr and Hf show similar incompatibility to Nb and Ta in all melts (Figure 4), which contradicts indications from previous studies that D_{Nb} and D_{Ta} should be higher than D_{Zr} and D_{Hf} (e.g., Bulatov et al., 2014; Hermann & Rubatto, 2009). Because Nb and Ta have higher valence (5+ versus 4+) and smaller ionic radii (64 and 62.5 versus 72 and 76 ppm; Tiepolo et al., 2000), Nb and Ta might be expected to be more incompatible (higher $D_{residue/melt}$). However, this is not seen because of anomalously high D values for Zr and Hf (Figure 4a). Second, as stated above, D_{MREE} and D_{HREE} in melts of pure sediment are considerably higher than in hybrid melts (Figure 4b), most likely because of buffering by residual almandine-rich garnet, which fractionates MREE and HREE more strongly than more magnesian garnet during melting (Figure 3a).

There is a positive correlation between Th/Yb and Nb/Yb ratios in all melts. Melts resulting from basalt-peridotite interaction have the lowest Th/Yb and highest Sm/Nd ratios, but, compared to fertile peridotite, the involvement of depleted peridotite clearly increases both Th/Yb and Nb/Yb fractionation, and also Sm/Nd fractionation (Figure 6). We attribute this change in elemental fractionation to the different residue mineral assemblages. Specifically, Rapp et al. (1999) found that orthopyroxene was present in experiments

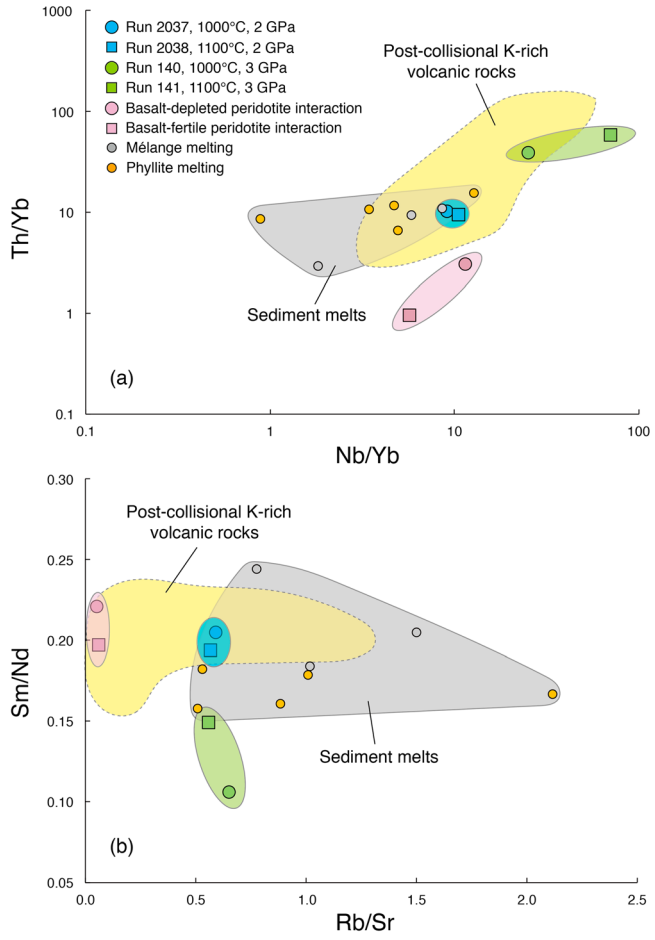

Figure 6. Variations of (a) Nb/Yb versus Th/Yb and (b) Rb/Sr versus Sm/Nd ratios of experimental melts compared to postcollisional K-rich volcanic rocks with K_2O of 3–5 wt% (data from Lustrino et al., 2011). Note the difference between direct melts of sediment (small circles) and hybrid melts (larger circles and squares). Data for basalt-depleted/fertile peridotite interaction from Rapp et al. (1999), mélange melting data from Castro et al. (2010), and phyllite melting data from Wang, Prelević, et al. (2017). All experiments plotted in this diagram are conducted on natural rocks.

with the depleted peridotite, but absent in experiments with the fertile peridotite; other than orthopyroxene, no phase assemblage difference was observed in their study. As the partition coefficients for orthopyroxene for HREE are substantially higher than for olivine (Adam & Green, 2006), high Th/Yb and Nb/Yb in the melts result.

In addition, melts resulting from basalt-peridotite interaction exhibit the lowest Rb/Sr ratios, indicating very similar partitioning ability for Rb and Sr during melting. All melts of sedimentary rocks plot at lower Nb/Yb than hybrid melts in Figure 6a, indicating that the hybridization process not only increases trace element concentrations but can also enhances Th/Yb and Nb/Yb fractionation. However, this feature is much less pronounced in Figure 6b where direct melts of sediment plot in between hybrid melts. It appears that sediment-peridotite interaction restricts Rb/Sr fractionation, because the Rb/Sr ratio is much greater in sediment melts (up to 2.0) than in hybrid melts (~0.5). Sm/Nd ratios are consistent for all melts (~0.15–0.25), implying relatively stable Sm/Nd fractionation regardless of whether or not peridotite is involved (Figure 6). Another intriguing feature is the strong effect exerted by pressure. Both Th/Yb and Nb/Yb fractionations are clearly augmented as pressure increases from 2 GPa to 3 GPa, whereas Sm/Nd fractionation exhibits an opposite trend. It is most likely due to the emergence of garnet in experiments at 3 GPa, which is believed to have low $D_{Th/Yb}$ and relatively high $D_{Sm/Nd}$ in many previous studies (e.g., Adam & Green, 2006; Green, 1994).

4.4. Implications for Melting of Recycled Continental Crust and K-Rich Magmatism From a Phlogopite-Free Source

Slab-derived melts or fluids produced during subduction rise to initiate metasomatic alteration of the overlying mantle wedge, which imparts several characteristic geochemical features to the subsequent magmas (e.g., Bebout & Barton, 1993; Stalder et al., 1998). Of particular significance, the sedimentary layer of the subducted oceanic crust can be transported into the subduction channel in the form of mélange that may also incorporate continental crustal fragments. This would interact with the peridotite and result in isotopic and trace element signatures of sediments being passed to ostensibly mantle-derived magmas.

Many K-rich postcollisional magmas owe their characteristic isotope and trace element features to the involvement of continental crust in the mantle source (Prelević et al., 2008, 2013; Tommasini et al., 2011; Wang, Prelević, et al., 2017). An ultra-depleted component in the source is also identified by presence of refractory Cr-spinel, high Fo olivine, and relatively low whole-rock FeO abundances and has been interpreted as forearc peridotite (Prelević & Foley, 2007). Therefore, the petrogenesis of K-rich postcollisional volcanism often appears to require interaction between the ultra-depleted peridotite and continental crust-derived sediment. Our experimental hybrid melts between continental crust-derived sediment and depleted peridotite exhibit high K_2O (up to 5.1 wt%) and Mg-number (up to 73), relatively low CaO (0.46–1.97 wt%) and Na_2O (0.92–2.31 wt%). Moreover, similar trace element patterns to those in our experimental hybrid melts are seen in postcollisional K-rich volcanic rocks with 3–5 wt% K_2O (Figure 7; Wang, Foley, et al., 2017). Trace elements exhibit almost identical arrays but with slightly lower concentrations in the experimental melts, which is interpreted as being due to either (i) the high sediment:peridotite mass ratio (1:1) used in the experiments or (ii) that the K-rich volcanic rocks plotted in Figure 7 have undergone fractionation, whereas experimental melts represent the primary, unfractionated starting point. Crust-mantle hybridization is required to produce the high Th/Yb versus Nb/Yb and relatively high Sm/Nd versus low Rb/Sr ratios seen in postcollisional K-rich volcanic rocks (Figure 6). Melting of neither sediment nor peridotite alone could produce such fractionation

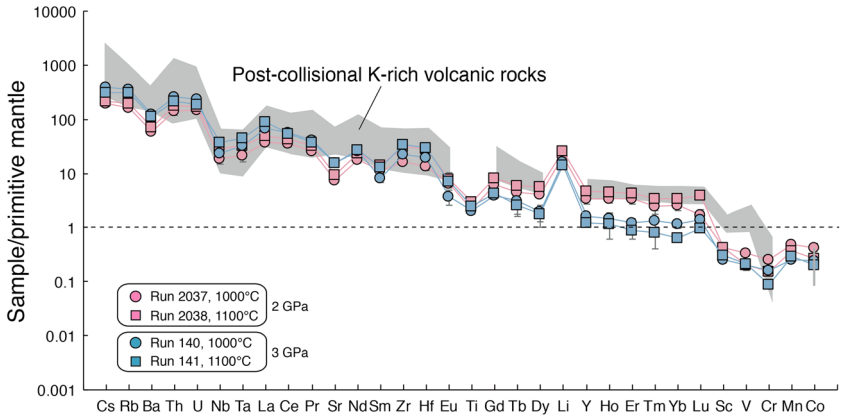

Figure 7. Primitive mantle normalized trace element compositions of experimental melts compared to postcollisional K-rich volcanic rocks with K_2O of 3–5 wt% (data from Lustrino et al., 2011). Patterns are similar but trace element concentrations are slightly lower in hybrid melts relative to postcollisional K-rich volcanic rocks. Primitive mantle values from Palme and O'Neill (2003).

features; it is only through sediment-peridotite hybridization with appropriate sediment:peridotite mass ratio that these characteristics could originate in postcollisional K-rich volcanic rocks.

This study demonstrates that potassium-rich melts can be produced in the absence of residual K-rich minerals such as phlogopite (Putirka et al., 2012; Wang, Foley, et al., 2017). Phlogopite has often been thought essential for the production of K-rich magmas (Condamine & Médard, 2014; Foley et al., 1996; Fritschle et al., 2013; Mallik et al., 2015; Prelević et al., 2012; Wyllie & Sekine, 1982), normally formed in the mantle wedge as a result of slab-derived fluid/melt migration in subduction zone and postcollisional settings. However, the absence of phlogopite in this study offers an alternative explanation, namely, that potassium is introduced from the subducted continental sediment via phengite, and not in either peridotite or in additional phlogopite-bearing ultramafic rocks as most previous studies have claimed (e.g., Foley, 1992, 1993; Prelević et al., 2008). Thus, phlogopite is not necessarily required in the source to produce magmas with moderately high K_2O contents (3–5 wt%). The lack of a coexisting potassium-rich mineral shows that potassium would be exclusively entrained into melts during slab-mantle hybridization at shallow depth, making them suitable metasomatizing agents in the mantle. Moreover, the potassium enrichment in melts (~4–5 wt% K_2O) concentrates K_2O relative to the content in the original phyllite (1.8 wt%). The only reasonable explanation is the breakdown of phengite in the phyllite, which is consumed completely and not transformed to other newly formed potassic minerals during melting. Subsequently, hybridized melts would take all the potassium released from the micas in the sediment (Wang, Foley, et al., 2017). The melting of phengite is made possible by postcollisional relaxation during which breaks in the slab and roll-back promote access of hot, upwelling asthenospheric mantle to cause melting in an imbricated assemblage of mixed phengite-bearing sediments and depleted forearc peridotite (Wang, Foley, et al., 2017; Wang, Prelević, et al., 2017).

We note here that although we propose that K-rich magmas can be produced from a phlogopite-free source, we do not claim that *all* K-rich magmas are produced without a role for phlogopite, particularly lamproites with extreme K_2O contents of 10 wt% or more. The hybrid melts produced in these experiments represent only the first stage of the hybridization process; these melts may further react with peridotite and cannot be expected to reach the surface in an unmodified state. It is thus logical that they are rare as magmas at the surface. Moreover, we envisage that a greater abundance of mica in the continent-derived sediment should lead to a greater volume of potassium-rich magmas.

5. Conclusions

In reaction experiments at 1000°, 2–3 GPa containing juxtaposed distinct blocks of peridotite and sediment, a reaction zone dominated by orthopyroxene occurred but with no analyzable hybrid melt, whereas large pools of hybrid melt were found in experiments in which peridotite and sediment were mixed before the experiments. The interaction between continental crustal sedimentary material and depleted peridotite

produces siliceous K-rich (~4–5 wt% K_2O) melt, with high contents of LILE and HFSE together with a considerable LREE preference over HREE. Garnets produced in metasediment melting experiments were relatively almandine rich, while those formed in hybridization melting experiments were enriched in pyrope. MREE and HREE showed much more pronounced compatibility in the residues of melting of the sedimentary rock than in hybrid melts, which indicated that the more siliceous melts of metasediment exert a greater effect on trace element distributions during sediment-peridotite interaction than does peridotite. Moreover, melts of sediment fractionate Rb strongly from Sr, whereas hybrid melts showed much less fractionation because of the diluting effect of peridotite. Th/Yb and Nb/Yb fractionation in melts of metasediment are enhanced by sediment-peridotite interaction.

The nearly identical trace element distribution pattern of hybrid melts and postcollisional K-rich volcanic rocks indicates that the petrogenesis of K-rich postcollisional volcanism is related to interaction between the ultra-depleted peridotite and continental crust-derived sediment. The absence of K-rich minerals, especially phlogopite, indicates that melts with K_2O contents as high as 4–5 wt% could be produced at shallow depths (50–80 km) via hybridization between continent-derived sediment and depleted peridotite without the need for residual phlogopite.

Acknowledgments
We are very grateful to Qing Xiong for providing dunite sample ZD11-53. Will Powell, David Adams, and Norman Pearson are appreciated for their help during laser and microprobe measurements. John Adam is warmly thanked for his supervision on piston-cylinder apparatus operation. We appreciate Ananya Mallik and Antonio Castro for their insightful reviews and the editorial support of Michael Walter. This work was supported by the Strategic Priority Research Program (B) of Chinese Academy of Sciences (grant XDB18000000), National Natural Science Foundation of China (grant 41773055), and the ARC Centre of Excellence for Core to Crust Fluid Systems/GEMOC. This is contribution 1163 from the ARC Centre of Excellence for Core to Crust Fluid Systems and 1126 in the GEMOC Key Centre. The Macquarie University HDR Fund supported experimental and analytical work. Three supplementary figures and all the data for this paper are available in supporting information S1.

References

Adam, J., & Green, T. (2006). Trace element partitioning between mica- and amphibole-bearing garnet lherzolite and hydrous basanitic melt: 1. Experimental results and the investigation of controls on partitioning behaviour. *Contributions to Mineralogy and Petrology*, *152*(1), 1–17. https://doi.org/10.1007/s00410-006-0085-4

Arculus, R. J., & Powell, R. (1986). Source component mixing in the regions of arc magma generation. *Journal of Geophysical Research*, *91*(B6), 5913–5926. https://doi.org/10.1029/JB091iB06p05913

Bebout, G. E., & Barton, M. D. (1993). Metasomatism during subduction: Products and possible paths in the Catalina Schist, California. *Chemical Geology*, *108*(1–4), 61–92. https://doi.org/10.1016/0009-2541(93)90318-D

Blundy, J. D., & Sparks, R. S. J. (1992). Petrogenesis of mafic inclusions in granitoids of the Adamello Massif, Italy. *Journal of Petrology*, *33*(5), 1039–1104. https://doi.org/10.1093/petrology/33.5.1039

Bodinier, J. I., Merlet, C., Bedini, R. M., Simien, F., Remaidi, M., & Garrido, C. J. (1996). Distribution of niobium, tantalum, and other highly incompatible trace elements in the lithospheric mantle: The spinel paradox. *Geochimica et Cosmochimica Acta*, *60*(3), 545–550. https://doi.org/10.1016/0016-7037(95)00431-9

Boyd, F. R., & England, J. L. (1960). Apparatus for phase-equilibrium measurements at pressures up to 50 kilobars and temperatures up to 1750°C. *Journal of Geophysical Research*, *65*(2), 741–748. https://doi.org/10.1029/JZ065i002p00741

Brenan, J. M., Finnigan, C. F., McDonough, W. F., & Homolova, V. (2012). Experimental constraints on the partitioning of Ru, Rh, Ir, Pt and Pd between chromite and silicate melt: The importance of ferric iron. *Chemical Geology*, *302*, 16–32.

Brey, G. P., & Köhler, T. (1990). Geothermobarometry in four-phase lherzolites II. New thermobarometers, and practical assessment of existing thermobarometers. *Journal of Petrology*, *31*(6), 1353–1378. https://doi.org/10.1093/petrology/31.6.1353

Bulatov, V. K., Brey, G. P., Girnis, A. V., Gerdes, A., & Höfer, H. E. (2014). Carbonated sediment-peridotite interaction and melting at 7.5–12 GPa. *Lithos*, *200-201*, 368–385. https://doi.org/10.1016/j.lithos.2014.05.010

Carlson, W. D. (2006). Dana lecture. Rates of Fe, Mg, Mn, and Ca diffusion in garnet. *American Mineralogist*, *91*(1), 1–11. https://doi.org/10.2138/am.2006.2043

Castro, A., & Gerya, T. V. (2008). Magmatic implications of mantle wedge plumes: Experimental study. *Lithos*, *103*(1–2), 138–148. https://doi.org/10.1016/j.lithos.2007.09.012

Castro, A., Gerya, T., Garcia-Casco, A., Fernandez, C., Diaz-Alvarado, J., Moreno-Ventas, I., & Low, I. (2010). Melting relations of MORB-sediment melanges in underplated mantle wedge plumes; implications for the origin of cordilleran-type batholiths. *Journal of Petrology*, *51*(6), 1267–1295. https://doi.org/10.1093/petrology/egq019

Chakraborty, S., & Ganguly, J. (1991). *Compositional zoning and cation diffusion in garnets, diffusion, atomic ordering, and mass transport* (pp. 120–175). New York: Springer.

Condamine, P., & Médard, E. (2014). Experimental melting of phlogopite-bearing mantle at 1 GPa: Implications for potassic magmatism. *Earth and Planetary Science Letters*, *397*(0), 80–92. https://doi.org/10.1016/j.epsl.2014.04.027

Conticelli, S., & Peccerillo, A. (1992). Petrology and geochemistry of potassic and ultrapotassic volcanism in central Italy: Petrogenesis and inferences on the evolution of the mantle sources. *Lithos*, *28*(3-6), 221–240. https://doi.org/10.1016/0024-4937(92)90008-M

Defant, M. J., & Drummond, M. S. (1990). Derivation of some modern arc magmas by melting of young subducted lithosphere. *Nature*, *347*(6294), 662–665. https://doi.org/10.1038/347662a0

Foley, S. (1992). Petrological characterization of the source components of potassic magmas: Geochemical and experimental constraints. *Lithos*, *28*(3-6), 187–204. https://doi.org/10.1016/0024-4937(92)90006-K

Foley, S. F. (1993). An experimental study of olivine lamproite: First results from the diamond stability field. *Geochimica et Cosmochimica Acta*, *57*(2), 483–489. https://doi.org/10.1016/0016-7037(93)90448-6

Foley, S. F., Jackson, S. E., Fryer, B. J., Greenouch, J. D., & Jenner, G. A. (1996). Trace element partition coefficients for clinopyroxene and phlogopite in an alkaline lamprophyre from Newfoundland by LAM-ICP-MS. *Geochimica et Cosmochimica Acta*, *60*(4), 629–638. https://doi.org/10.1016/0016-7037(95)00422-X

Foley, S. F., & Pintér, Z. (2018). Primary melt compositions in the Earth's mantle. In Y. Kono & C. Sanloup (Eds.), *Magmas Under Pressure: Advances in High-Pressure Experiments on Structure and Properties of Melts* (chap. 1, pp. 3–42). Amsterdam: Elsevier.

Fritschle, T., Prelevic, D., Foley, S. F., & Jacob, D. E. (2013). Petrological characterization of the mantle source of Mediterranean lamproites: Indications from major and trace elements of phlogopite. *Chemical Geology*, *353*, 267–279. https://doi.org/10.1016/j.chemgeo.2012.09.006

Green, T. H. (1994). Experimental studies of trace-element partitioning applicable to igneous petrogenesis—Sedona 16 years later. *Chemical Geology*, *117*(1–4), 1–36. https://doi.org/10.1016/0009-2541(94)90119-8

Green, T. H., Blundy, J. D., Adam, J., & Yaxley, G. M. (2000). SIMS determination of trace element partition coefficients between garnet, clinopyroxene and hydrous basaltic liquids at 2–7.5 GPa and 1080–1200°C. *Lithos*, *53*(3-4), 165–187. https://doi.org/10.1016/S0024-4937(00)00023-2

Green, T. H., Ringwood, A. E., & Major, A. (1966). Friction effects and pressure calibration in a piston-cylinder apparatus at high pressure and temperature. *Journal of Geophysical Research*, *71*(14), 3589–3594. https://doi.org/10.1029/JZ071i014p03589

Glaser, S. M., Foley, S. F., & Günther, D. (1999). Trace element compositions of minerals in garnet and spinel peridotite xenoliths from the Vitim volcanic field, Transbaikalia, eastern Siberia. *Lithos*, *48*(1–4), 263–285. https://doi.org/10.1016/S0024-4937(99)00032-8

Hauri, E. H., Wagner, T. P., & Grove, T. L. (1994). Experimental and natural partitioning of Th, U, Pb and other trace elements between garnet, clinopyroxene and basaltic melts. *Chemical Geology*, *117*(1–4), 149–166. https://doi.org/10.1016/0009-2541(94)90126-0

Hermann, J., & Rubatto, D. (2009). Accessory phase control on the trace element signature of sediment melts in subduction zones. *Chemical Geology*, *265*(3–4), 512–526. https://doi.org/10.1016/j.chemgeo.2009.05.018

Hermann, J., & Spandler, C. J. (2007). Sediment melts at sub-arc depths: An experimental study. *Journal of Petrology*, *49*(4), 717–740.

Hickmott, D. D., Shimizu, N., Spear, F. S., & Selverstone, J. (1987). Trace-element zoning in a metamorphic garnet. *Geology*, *15*(6), 573–576. https://doi.org/10.1130/0091-7613(1987)15%3C573:TZIAMG%3E2.0.CO;2

Horn, I., Foley, S. F., Jackson, S. E., & Jenner, G. A. (1994). Experimentally determined partitioning of high field strength and selected transition elements between spinel and basaltic melts. *Chemical Geology*, *117*(1-4), 193–218. https://doi.org/10.1016/0009-2541(94)90128-7

Johnson, K. T. M. (1998). Experimental determination of partition coefficients for rare earth and high-field-strength elements between clinopyroxene, garnet, and basaltic melt at high pressures. *Contributions to Mineralogy and Petrology*, *133*(1–2), 60–68. https://doi.org/10.1007/s004100050437

Johnston, A. D., & Schwab, B. E. (2004). Constraints on clinopyroxene/melt partitioning of REE, Rb, Sr, Ti, Cr, Zr, and Nb during mantle melting: First insights from direct peridotite melting experiments at 1.0 GPa. *Geochimica et Cosmochimica Acta*, *68*(23), 4949–4962. https://doi.org/10.1016/j.gca.2004.06.009

Johnston, A. D., & Wyllie, P. J. (1989). The system tonalite-peridotite-H_2O at 30 kbar, with applications to hybridization in subduction zone magmatism. *Contributions to Mineralogy and Petrology*, *102*(3), 257–264. https://doi.org/10.1007/BF00373719

Kay, R. W. (1980). Volcanic arc magmas: Implications of a melting-mixing model for element recycling in the crust-upper mantle system. *The Journal of Geology*, *88*(5), 497–522. https://doi.org/10.1086/628541

Kelemen, P. B., Shimizu, N., & Dunn, T. (1993). Relative depletion of niobium in some arc magmas and the continental crust: Partitioning of K, Nb, La and Ce during melt/rock reaction in the upper mantle. *Earth and Planetary Science Letters*, *120*(3–4), 111–134. https://doi.org/10.1016/0012-821X(93)90234-Z

Lee, C.-T. A., Harbert, A., & Leeman, W. P. (2007). Extension of lattice strain theory to mineral/mineral rare-earth element partitioning: An approach for assessing disequilibrium and developing internally consistent partition coefficients between olivine, orthopyroxene, clinopyroxene and basaltic melt. *Geochimica et Cosmochimica Acta*, *71*(2), 481–496. https://doi.org/10.1016/j.gca.2006.09.014

Lustrino, M., Duggen, S., & Rosenberg, C. L. (2011). The central-western Mediterranean: Anomalous igneous activity in an anomalous collisional tectonic setting. *Earth-Science Reviews*, *104*(1-3), 1–40. https://doi.org/10.1016/j.earscirev.2010.08.002

Martin, A. M., Laporte, D., Koga, K. T., Kawamoto, T., & Hammouda, T. (2012). Experimental study of the stability of a dolomite + coesite assemblage in contact with peridotite: Implications for sediment–mantle interaction and diamond formation during subduction. *Journal of Petrology*, *53*(2), 391–417. https://doi.org/10.1093/petrology/egr066

McDonough, W. F., Stosch, H. G., & Ware, N. G. (1992). Distribution of titanium and the rare earth elements between peridotitic minerals. *Contributions to Mineralogy and Petrology*, *110*(2–3), 321–328. https://doi.org/10.1007/BF00310747

McLennan, S. M. (2001). Relationships between the trace element composition of sedimentary rocks and upper continental crust. *Geochemistry, Geophysics, Geosystems*, *2*(4), 203–236.

Mallik, A., & Dasgupta, R. (2012). Reaction between MORB-eclogite derived melts and fertile peridotite and generation of ocean island basalts. *Earth and Planetary Science Letters*, *329-330*(0), 97–108. https://doi.org/10.1016/j.epsl.2012.02.007

Mallik, A., & Dasgupta, R. (2013). Reactive infiltration of MORB-Eclogite-derived carbonated silicate melt into fertile peridotite at 3 GPa and genesis of alkalic magmas. *Journal of Petrology*, *54*(11), 2267–2300. https://doi.org/10.1093/petrology/egt047

Mallik, A., & Dasgupta, R. (2014). Effect of variable CO_2 on eclogite-derived andesite and lherzolite reaction at 3 GPa—Implications for mantle source characteristics of alkalic ocean island basalts. *Geochemistry, Geophysics, Geosystems*, *15*, 1533–1557. https://doi.org/10.1002/2014GC005251

Mallik, A., Dasgupta, R., Tsuno, K., & Nelson, J. (2016). Effects of water, depth and temperature on partial melting of mantle-wedge fluxed by hydrous sediment-melt in subduction zones. *Geochimica et Cosmochimica Acta*, *195*(2016), 226–243. https://doi.org/10.1016/j.gca.2016.08.018

Mallik, A., Nelson, J., & Dasgupta, R. (2015). Partial melting of fertile peridotite fluxed by hydrous rhyolitic melt at 2–3 GPa: Implications for mantle wedge hybridization by sediment melt and generation of ultrapotassic magmas in convergent margins. *Contributions to Mineralogy and Petrology*, *169*(5), 1–24.

Morimoto, N. (1988). Nomenclature of pyroxenes. *Mineralogy and Petrology*, *39*(1), 55–76. https://doi.org/10.1007/BF01226262

Murphy, D. T., Collerson, K. D., & Kamber, B. S. (2002). Lamproites from Gaussberg, Antarctica: Possible transition zone melts of Archaean subducted sediments. *Journal of Petrology*, *43*(6), 981–1001. https://doi.org/10.1093/petrology/43.6.981

Melzer, S., & Foley, S. F. (2000). Phase relations and fractionation sequences in potassic magma series modelled in the system $CaMgSi_2O_6$-$KAlSiO_4$-Mg_2SiO_4-SiO_2-F_2O_{-1} at 1 bar and 18 kbar. *Contributions to Mineralogy and Petrology*, *138*(2), 186–197. https://doi.org/10.1007/s004100050017

Nash, W. P., & Crecraft, H. R. (1985). Partition coefficients for trace elements in silicic magmas. *Geochimica Et Cosmochimica Acta*, *49*(11), 2309–2322.

Nicholls, I. A., & Ringwood, A. E. (1973). Effect of water on olivine stability in tholeiites and the production of silica-saturated magmas in the island-arc environment. *The Journal of Geology*, *81*(3), 285–300. https://doi.org/10.1086/627871

Nielsen, R. L., Forsythe, L. M., Gallahan, W. E., & Fisk, M. R. (1994). Major- and trace-element magnetite-melt equilibria. *Chemical Geology*, *117*(1-4), 167–191. https://doi.org/10.1016/0009-2541(94)90127-9

Nielsen, R. L., Gallahan, W. E., & Newberger, F. (1992). Experimentally determined mineral-melt partition coefficients for Sc, Y and REE for olivine, orthopyroxene, pigeonite, magnetite and ilmenite. *Contributions to Mineralogy and Petrology*, *110*(4), 488–499. https://doi.org/10.1007/BF00344083

Page, P., & Barnes, S. J. (2009). Using trace elements in chromites to constrain the origin of podiform chromitites in the Thetford Mines Ophiolite, Quebec, Canada. *Economic Geology*, *104*(7), 997–1018. https://doi.org/10.2113/econgeo.104.7.997

Peccerillo, A., & Martinotti, G. (2006). The western Mediterranean lamproitic magmatism: Origin and geodynamic significance. *Terra Nova*, *18*(2), 109–117. https://doi.org/10.1111/j.1365-3121.2006.00670.x

Peccerillo, A., Poli, G., & Serri, G. (1988). Petrogenesis of orenditic and kamafugitic rocks from Central Italy. *Canadian Mineralogist*, *26*, 45–65.

Pertermann, M., Hirschmann, M. M., Hametner, K., Günther, D., & Schmidt, M. W. (2004). Experimental determination of trace element partitioning between garnet and silica-rich liquid during anhydrous partial melting of MORB-like eclogite. *Geochemistry, Geophysics, Geosystems*, *5*, Q05A01. https://doi.org/10.1029/2003GC000638

Palme, H., & O'Neill, H. S. C. (2003). Cosmochemical estimates of mantle composition. *Treatise on Geochemistry*, *2*, 1–38.

Plank, T., & Langmuir, C. H. (1998). The chemical composition of subducting sediment and its consequences for the crust and mantle. *Chemical Geology*, *145*(3–4), 325–394. https://doi.org/10.1016/S0009-2541(97)00150-2

Prelević, D., & Foley, S. F. (2007). Accretion of arc-oceanic lithospheric mantle in the Mediterranean: Evidence from extremely high-Mg olivines and Cr-rich spinel inclusions in lamproites. *Earth and Planetary Science Letters*, *256*(1–2), 120–135. https://doi.org/10.1016/j.epsl.2007.01.018

Prelević, D., Foley, S. F., Romer, R., & Conticelli, S. (2008). Mediterranean Tertiary lamproites derived from multiple source components in postcollisional geodynamics. *Geochimica et Cosmochimica Acta*, *72*(8), 2125–2156. https://doi.org/10.1016/j.gca.2008.01.029

Prelević, D., Foley, S. F., Romer, R. L., Cvetković, V., & Downes, H. (2005). Tertiary ultrapotassic volcanism in Serbia: Constraints on petrogenesis and mantle source characteristics. *Journal of Petrology*, *46*(7), 1443–1487. https://doi.org/10.1093/petrology/egi022

Prelević, D., Jacob, D. E., & Foley, S. F. (2013). Recycling plus: A new recipe for the formation of Alpine-Himalayan orogenic mantle lithosphere. *Earth and Planetary Science Letters*, *362*, 187–197. https://doi.org/10.1016/j.epsl.2012.11.035

Prelević, D., Akal, C., Foley, S. F., Romer, R. L., Stracke, A., & van den Bogaard, P. (2012). Ultrapotassic mafic rocks as geochemical proxies for post-collisional dynamics of orogenic lithospheric mantle: The case of southwestern Anatolia, Turkey. *Journal of Petrology*, *53*(5), 1019–1055. https://doi.org/10.1093/petrology/egs008

Prouteau, G., Scaillet, B., Pichavant, M., & Maury, R. (2001). Evidence for mantle metasomatism by hydrous silicic melts derived from subducted oceanic crust. *Nature*, *410*(6825), 197–200. https://doi.org/10.1038/35065583

Putirka, K., Jean, M., Cousens, B., Sharma, R., Torrez, G., & Carlson, C. (2012). Cenozoic volcanism in the Sierra Nevada and Walker Lane, California, and a new model for lithosphere degradation. *Geosphere*, *8*(2), 265–291. https://doi.org/10.1130/GES00728.1

Rapp, R. P., Shimizu, N., Norman, M. D., & Applegate, G. S. (1999). Reaction between slab-derived melts and peridotite in the mantle wedge: Experimental constraints at 3.8 GPa. *Chemical Geology*, *160*(4), 335–356. https://doi.org/10.1016/S0009-2541(99)00106-0

Sekine, T., & Wyllie, P. (1982a). Phase relationships in the system $KAlSiO_4$-Mg_2SiO_4-SiO_2-H_2O as a model for hybridization between hydrous siliceous melts and peridotite. *Contributions to Mineralogy and Petrology*, *79*(4), 368–374. https://doi.org/10.1007/BF01132066

Sekine, T., & Wyllie, P. J. (1982b). Synthetic systems for modeling hybridization between hydrous siliceous magmas and peridotite in subduction zones. *The Journal of Geology*, *90*(6), 734–741. https://doi.org/10.1086/628728

Sekine, T., & Wyllie, P. J. (1982c). The system granite-peridotite-H_2O at 30 kbar, with applications to hybridization in subduction zone magmatism. *Contributions to Mineralogy and Petrology*, *81*(3), 190–202. https://doi.org/10.1007/BF00371296

Sekine, T., & Wyllie, P. J. (1983). Experimental simulation of mantle hybridization in subduction zones. *The Journal of Geology*, *91*(5), 511–528. https://doi.org/10.1086/628802

Shimizu, N., & Kushiro, I. (1975). The partitioning of rare earth elements between garnet and liquid at high pressures: Preliminary experiments. *Geophysical Research Letters*, *2*(10), 413–416. https://doi.org/10.1029/GL002i010p00413

Skora, S., & Blundy, J. (2010). High-pressure hydrous phase relations of radiolarian clay and implications for the involvement of subducted sediment in arc magmatism. *Journal of Petrology*, *51*(11), 2211–2243. https://doi.org/10.1093/petrology/egq054

Stosch, H. G. (1982). Rare earth element partitioning between minerals from anhydrous spinel peridotite xenoliths. *Geochimica et Cosmochimica Acta*, *46*(5), 793–811. https://doi.org/10.1016/0016-7037(82)90031-X

Stalder, R., Foley, S. F., Brey, G. P., & Horn, I. (1998). Mineral-aqueous fluid partitioning of trace elements at 900-1200°C and 3.0–5.7 GPa: New experimental data for garnet, clinopyroxene, and rutile, and implications for mantle metasomatism. *Geochimica et Cosmochimica Acta*, *62*(10), 1781–1801. https://doi.org/10.1016/S0016-7037(98)00101-X

Tatsumi, Y. (2001). Geochemical modeling of partial melting of subducting sediments and subsequent melt-mantle interaction: Generation of high-Mg andesites in the Setouchi volcanic belt, southwest Japan. *Geology*, *29*(4), 323–326. https://doi.org/10.1130/0091-7613(2001)029%3C0323:GMOPMO%3E2.0.CO;2

Tatsumi, Y., Hamilton, D. L., & Nesbitt, R. W. (1986). Chemical characteristics of fluid phase released from a subducted lithosphere and origin of arc magmas: Evidence from high-pressure experiments and natural rocks. *Journal of Volcanology and Geothermal Research*, *29*(1-4), 293–309. https://doi.org/10.1016/0377-0273(86)90049-1

Taylor, S. R., & McLennan, S. M. (1995). The geochemical evolution of the continental crust. *Reviews of Geophysics*, *33*(2), 241–265. https://doi.org/10.1029/95RG00262

Thomsen, T. B., & Schmidt, M. W. (2008). The biotite to phengite reaction and mica-dominated melting in fluid + carbonate-saturated pelites at high pressures. *Journal of Petrology*, *49*(10), 1889–1914. https://doi.org/10.1093/petrology/egn051

Tiepolo, M., Vannucci, R., Oberti, R., Foley, S., Bottazzi, P., & Zanetti, A. (2000). Nb and Ta incorporation and fractionation in titanian pargasite and kaersutite: Crystal–chemical constraints and implications for natural systems. *Earth and Planetary Science Letters*, *176*(2), 185–201. https://doi.org/10.1016/S0012-821X(00)00004-2

Tommasini, S., Avanzinelli, R., & Conticelli, S. (2011). The Th/La and Sm/La conundrum of the Tethyan realm lamproites. *Earth and Planetary Science Letters*, *301*(3–4), 469–478. https://doi.org/10.1016/j.epsl.2010.11.023

van Westrenen, W., Blundy, J. D., & Wood, B. J. (2001). High field strength element/rare earth element fractionation during partial melting in the presence of garnet: Implications for identification of mantle heterogeneities. *Geochemistry, Geophysics, Geosystems*, *2*(7), 223–235.

Wang, Y., Foley, S. F., & Prelević, D. (2017). Potassium-rich magmatism from a phlogopite-free source. *Geology*, *45*(5), 467–470. https://doi.org/10.1130/G38691.1

Wang, Y., Prelević, D., Buhre, S., & Foley, S. F. (2017). Constraints on the sources of post-collisional K-rich magmatism: The roles of continental clastic sediments and terrigenous blueschists. *Chemical Geology*, *455*, 192–207. https://doi.org/10.1016/j.chemgeo.2016.10.006

Wyllie, P., & Sekine, T. (1982). The formation of mantle phlogopite in subduction zone hybridization. *Contributions to Mineralogy and Petrology*, *79*(4), 375–380. https://doi.org/10.1007/BF01132067